Published in final edited form as:
J Biomed Opt. 2008 ; 13(4): 044041. doi:10.1117/1.2966122.

Antibody-labeled fluorescence imaging of dendritic cell populations *in vivo*

Ryan J. Cummings[1,*], **Soumya Mitra**[2,*], **Edith M. Lord**[1], and **Thomas H. Foster**[2]

1*Department of Microbiology and Immunology, University of Rochester Medical Center, Rochester, NY 14642*

2*Department of Imaging Sciences, University of Rochester Medical Center, Rochester, NY 14642*

Abstract

We report an optical molecular imaging technique that exploits local administration of fluorophore-conjugated antibodies and confocal fluorescence microscopy to achieve high contrast imaging of host cell populations in normal and tumor tissue in living mice. The method achieves micron-scale spatial resolution to depths greater than 100 μm. We illustrate the capabilities of this approach by imaging two dendritic cell populations in the skin and normal and tumor vasculature *in vivo*.

Keywords

In vivo imaging; immune cell imaging; confocal microscopy

Noninvasive imaging offers critically important windows into cell and tissue structure and function, normal and diseased physiology, and responses to therapeutic intervention. An explosion of imaging methods has occurred in recent decades, and applications span a wide range of biomedical specialties. Optical imaging, while limited with respect to the depths it can probe, offers exquisite spatial resolution and molecular specificity. *In vivo* applications of optical coherence and fluorescence tomography, reflectance and fluorescence confocal imaging, and multi-photon imaging are all undergoing rapid expansion (1,2). Biologically important optical signals arise from endogenous chromophores and light-matter interactions (3) and from exogenously administered labels targeting molecular or cellular structure or function (4,5).

Trafficking of immune cells in normal and malignant tissue is an area of intense interest, in which conventional technologies such as immunohistochemistry have provided extensive information. New *in vivo* techniques based on intravital confocal and multiphoton microscopy have revealed amazing images of immune cell interactions, such as those between antigen presenting dendritic cells and T cells, in surgically exposed lymph nodes (6-9). Exploiting the unique morphology of dendritic cells (DCs), a recent study reported the use of reflectance confocal microscopy to image the distribution of epithelial DCs in human cornea *in vivo* (10). Langerhans cells (LC) and other DCs in the skin are important as they are often the first to encounter antigen. These cells are of particular consideration from an imaging standpoint in that they are directly accessible via optical methods.

Correspondence to: Thomas H. Foster, Department of Imaging Sciences, 601 Elmwood Ave., Box 648, Rochester, NY 14642, Tel: 585-275-1347, Email: thomas.foster@rochester.edu.
*These two authors contributed equally to this work.

Recently, we demonstrated a fresh whole mount immunolabeling method that enables multi-color imaging of tumor and normal tissue vasculature and lymphatics, host cell populations, and extracellular matrix with minimal perturbation of tissue architecture (11). Here we describe the extension of a fluorophore-conjugated-antibody-labeling-based confocal fluorescence imaging method to living mice and use the technique to identify LC and dermal or interstitial DC (iDC) trafficking in normal ear and in an intradermal murine tumor model. Within 2 h after direct intradermal injection of antibody, the method yields images with very high contrast and confocal image resolution to depths of at least 100 μm in living tissue. Excellent staining persists for a minimum of 3 – 6 h following a single injection. Although these two DC populations are labeled using the same antibody directed against the major histocompatibility complex class II (MHC-II), they are distinguished unambiguously on the basis of their distinct morphologies and their stratification in the epidermal and dermal layers of the skin (12).

Prior to injection of fluorophore-conjugated antibodies, hair on the ears of BALB/c mice was removed by a chemical depilatory agent. One day after hair removal, mice were anesthetized and ears were injected intradermally on the ventral side with 40 μl of an antibody cocktail consisting of phosphate buffered saline (PBS), Fc block (0.35 mg/ml) (BD Biosciences, San Diego, CA), allophycocyanin (APC)-conjugated anti(α)MHC-II (0.05 mg/ml) (eBioscience, Inc. San Diego, CA), and AlexaFluor488-conjugated αCD31 (0.05 mg/ml) (Biolegend, San Diego, CA). The first of these antibodies labels the two morphologically distinct yet related antigen presenting cells - the LCs within the epidermis and iDCs in the dermis (10); the second labels the adhesion molecule PECAM, which is highly expressed on blood vessels and less intensely on lymphatic vessels. Vessels reside only in the dermal layer, and labeling them contributes to the identification of the two DC populations. After 2 h to allow for the unlabeled antibody to clear, mice were again anesthetized for imaging.

In vivo imaging was performed using a custom inverted laser scanning confocal fluorescence microscope (13,14). We have recently reported on the use of the antibody labeling technique in conjunction with the confocal imaging system to visualize the intratumor distribution of a photodynamic therapy sensitizer *in vivo* with respect to fluorophore-labeled CD31-positive vessels (15). In this study, to image the two DC populations and CD31-positive vessels we used sequential two-color excitation of identical fields of view; APC was excited with a 639 nm diode laser and Alexa488 was excited with 488 nm from an argon ion laser. The APC and Alexa488 emissions were detected using a 647LP long pass filter and a 515/30 band pass filter, respectively. The combination of a 100 μm diameter pinhole and a 10×, 0.45 NA objective gave an optical section thickness of approximately 6 μm as determined by fluorescence edge response measurements (13). The images were acquired with a lateral resolution of 1 μm per pixel. Mice were placed on the stage in the supine position so the ventral side of the ear was facing downward for imaging. Confocal images were then acquired every 3 μm beginning at an initial depth of roughly 30 μm from the surface. The images could then be analyzed individually or as a three-dimensional volume. For all experiments, the appropriate isotype controls were used to rule out non-specific staining.

Confocal fluorescence images obtained *in vivo* show positive staining for both DC types as evident by their unique morphologies at depths consistent with their localization in epidermal or dermal layers. Within the epidermis at a depth of approximately 40 μm from the surface of the ear, an extensive mesh-network of densely packed LCs with characteristic long dendritic-like projections (12) is shown in Fig. 1(a). Optical sections acquired in the dermis at depths of approximately 80 μm (Fig. 1(b)) show that the LC population is no longer present and that it is replaced by a stout, relatively sparse iDC population lacking long projections. Also evident in Fig. 1(b) and exclusive to the dermis is the extensive vasculature system, which is labeled with αCD31 antibody and which serves as a useful bio-marker to discriminate dermal from epidermal layers. We note that the iDCs tend to cluster tightly in the vicinity of the vasculature.

To confirm the identification of the DC populations imaged *in vivo*, we used whole-mount labeling of *ex vivo* tissues obtained from the dermal and epidermal layers of the ear and conventional fluorescence microscopy. Although both LCs and iDCs are MHC-II positive on their cell surfaces, only the LCs are positive for internal langerin, a C-type lectin unique to the cell and crucial for its development (16). Briefly, mice were sacrificed, ear hair was chemically removed, and ears were excised and split with the aid of forceps into dorsal and ventral halves. For dermal labeling, split ears were placed in 200 μl of PBS with Fc Block (28.6 μg/ml), APC-conjugated αMHC-II (7.5 μg/ml), phycoerythrin (PE)-conjugated αCD31 (7.5 μg/ml) and stained for 2 h at 4°C. To label the epidermis exclusively, additional tissue processing was required. Following ear splitting, halves were floated in 0.5 M ammonium thiocyanate at 37° C for 20 minutes to separate epidermal from dermal layers. The epidermal layer was then fixed in 2% paraformaldehyde at room temperature for 15 minutes to permeabilize the cells to enable labeling of internal langerin. Epidermal tissue was then incubated for 2 h with PE-conjugated αlangerin (7.5 μg/ml) and APC-conjugated αMHC-II (7.5 μg/ml). Positive staining of epidermal whole mounts with both αMHC-II (Fig. 1(c)) and internal αlangerin (Fig. 1(d)) confirms the identification of these epidermal LCs. This critical confirmation can only be performed *ex vivo*, as cell permeabilization is not possible *in vivo*. The significant overlap between the images of the cell surface and internal markers for LCs is depicted in Fig. 1(e). Single-color control experiments revealed no detectable cross talk between these two detection channels. The long cellular processes characteristic of these LCs are apparent in both the images obtained from the epidermal whole mount preparation and from the superficial optical sections *in vivo* (Fig. 1(a)). *Ex vivo* fluorescence imaging of the dermal layer (Fig. 1(f)) reveals vascular and DC cell morphology features similar to those observed in the images obtained from the deeper, dermal skin layer *in vivo* (Fig. 1(b)).

We have also implemented this technique to examine the tumor microenvironment in EMT6 mammary tumors grown intradermally in the ears of BALB/c mice. Tumors were initiated with an intradermal injection of 2×10^5 EMT6 cells and grown to a diameter of approximately 3 mm. MHC-II$^+$ cells and tumor blood vessels were labeled with APC-conjugated αMHC-II and Alexa488-conjugated αCD31, respectively, using intradermal injection of the antibody cocktail described above. As illustrated in Fig. 2, *in vivo* confocal images acquired at two different depths 2 h after antibody administration revealed excellent, high-contrast staining of MHC-II$^+$ cells. Specifically, the signal levels from stained cells observed in Figs. 2(a) and 2(c) are at least 4-8-fold higher than the adjacent background. Images acquired at 40 μm below the surface (Fig. 2(a) and (b)) reveal a population of epidermal LCs morphologically similar to those seen in Fig. 1(a) and 1(c). In comparison to the DCs imaged at a comparable depth in the normal ear (Figs. 1(b) and 1(f)), at a depth of 80 μm in the tumor (Fig. 2(c) and (d)), the MHC-II$^+$ cells are more numerous, their distribution is more diffuse, and their morphologies suggest a mixed population that may include not only LCs and iDCs similar to the normal ear but also macrophages. The deeper image also shows the CD31-positive tumor vasculature.

We note that the field-of-view of the *in vivo* images of Figs. 2(a) and 2(c) is 800 μm × 800 μm and that antibody labeling of MHC-II and CD31 is efficient across the entire image following a single injection outside of the imaging field. Thus, the antibody conjugates diffused laterally a distance of more than 800 μm, which is much greater than the maximum depth at which quality images can be obtained with single photon excited confocal fluorescence imaging. The method is not therefore limited by the depth of antibody diffusion but rather by attenuation of the excitation light. We note also that both DC populations are fully accessible to our imaging method in the mouse ear. This has been confirmed by successfully imaging CD31-positive vessels at depths of approximately 125 μm, roughly 25 μm beyond the layer where the iDCs are stratified in the normal ear (data not shown).

The ability to image noninvasively specific cell types at high spatial resolution *in vivo* and the availability of a wide variety of fluorescently conjugated antibodies render this technique very attractive for many applications in immunology and tumor biology. A particular advantage of intradermal vs. systemic injection (4) is that it requires the use of significantly less antibody, and it can be performed with standard, commercially available antibody preparations with negligible toxicity as compared to that encountered from systemic administration.

Acknowledgements

The authors acknowledge support from NIH grants CA28332, UI9AI067733, and CA68409.

References

1. Ntziachristos V. Fluorescence molecular imaging. Annu Rev Biomed Eng 2006;8:1–33. [PubMed: 16834550]
2. Yun SH, Tearney GJ, Vakoc BJ, Shishkov M, Oh WY, Desjardins AE, Suter MJ, Chan RC, Evans JA, Jang IK, Nishioka NS, de Boer JF, Bouma BE. Comprehensive volumetric optical microscopy in vivo. Nat Med 2006;12:1429–1433. [PubMed: 17115049]
3. Brown E, McKee T, diTomaso E, Pluen A, Seed B, Boucher Y, Jain RK. Dynamic imaging of collagen and its modulation in tumors in vivo using second-harmonic generation. Nat Med 2003;9:796–801. [PubMed: 12754503]
4. Sipkins DA, Wei X, Wu JW, Runnels JM, Côté D, Means TK, Luster AD, Scadden DT, Lin CP. In vivo imaging of specialized bone marrow endothelial microdomains for tumour engraftment. Nature 2005;435:969–973. [PubMed: 15959517]
5. Runnels JM, Zamiri P, Spencer JA, Veilleux I, Wei X, Bogdanov A, Lin CP. Imaging molecular expression on vascular endothelial cells by in vivo immunofluorescence microscopy. Mol Imaging 2006;5:31–40. [PubMed: 16779968]
6. Stoll S, Delon J, Brotz TM, Germain RN. Dynamic imaging of T cell-dendritic cell interactions in lymph nodes. Science 2002;296:1873–1876. [PubMed: 12052961]
7. Miller MJ, Wei SH, Cahalan MD, Parker I. Autonomous T cell trafficking examined in vivo with intravital two-photon microscopy. Proc Natl Acad Sci USA 2003;100:2604–2609. [PubMed: 12601158]
8. Germain RN, Miller MJ, Dustin ML, Nussenzweig MC. Dynamic imaging of the immune system: progress, pitfalls and promise. Nat Rev Immunol 2006;6:497–507. [PubMed: 16799470]
9. Sumen C, Mempel TR, Mazo IB, von Andrian UH. Intravital microscopy: visualizing immunity in context. Immunity 2004;21:315–329. [PubMed: 15357943]
10. Mastropasqua L, Nubile M, Lanzini M, Carpineto P, Ciancaglini M, Pannellini T, Di Nicola M, Dua HS. Epithelial dendritic cell distribution in normal and inflamed human cornea: in vivo confocal microscopy study. Am J Ophthalmol 2006;142:736–744. [PubMed: 17056357]
11. Gerber SA, Rybalko VY, Bigelow CE, Lugade AA, Foster TH, Frelinger JG, Lord EM. Preferential attachment of peritoneal tumor metastases to omental immune aggregates and possible role of a unique vascular microenvironment in metastatic survival and growth. Am J Pathol 2006;169:1739–1752. [PubMed: 17071597]
12. Valladeau J, Saeland S. Cutaneous dendritic cells. Semin Immunol 2005;17:273–283. [PubMed: 15953735]
13. Bigelow CE, Harkrider CJ, Conover DL, Foster TH, Georgakoudi I, Mitra S, Nichols MG, Rajadhyaksha M. Retrofitted confocal laser scanner for a commercial inverted fluorescence microscope. Rev Sci Instrum 2001;72:3407–3410.
14. Bigelow CE, Conover DL, Foster TH. Confocal fluorescence spectroscopy and anisotropy imaging system. Opt Lett 2003;28:695–697. [PubMed: 12747710]
15. Mitra S, Foster TH. In vivo confocal fluorescence imaging of the intratumor distribution of the photosensitizer mono-L-aspartylchlorin-e6. Neoplasia 2008;10:429–438. [PubMed: 18472960]
16. Valladeau J, Ravel O, Dezutter-Dambuyant C, Moore K, Kleijmeer M, Liu Y, Duvert-Frances V, Vincent C, Schmitt D, Davoust J, Caux C, Lebecque S, Saeland S. Langerin, a novel C-type lectin

specific to Langerhans cells, is an endocytic receptor that induces the formation of Birbeck granules. Immunity 2000;12:71–81. [PubMed: 10661407]

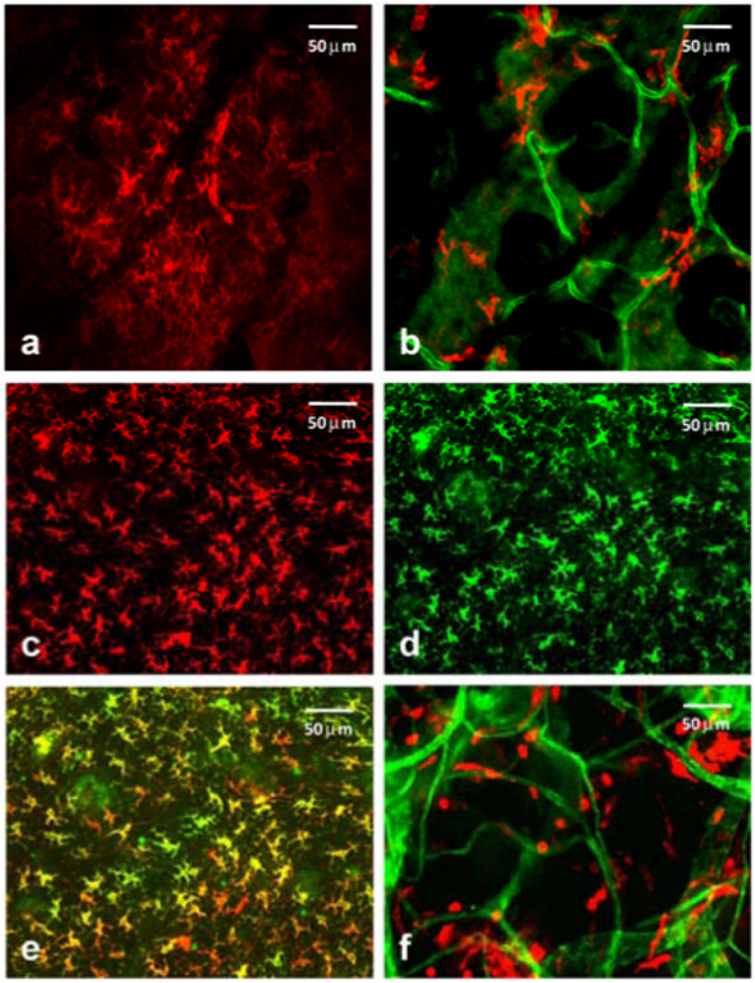

Figure 1.

In vivo confocal fluorescence images of MHC-II$^+$ cells in the mouse ear reveal two morphologically distinct cutaneous DC populations in superficial epidermal (a) and deeper dermal (b) layers of the tissue. In (b) dermal vessels are labeled with Alexa488-conjugated αCD31. (c-f) *Ex vivo* whole-mount histology confirms *in vivo* observations. Excised ears were split and processed; epidermis was stained with αMHC-II (c) and αlangerin (d) to confirm the identification and morphology of Langerhans cells. Image overlay (e) confirms the dual staining. (f) DCs in the dermis were stained with αMHC-II (red), and their distribution relative to αCD31-labeled vessels (green) is shown. These findings were confirmed in 10 and 20 mice for *in vivo* confocal and whole-mount imaging, respectively. The field of view in all images is 380 μm × 380 μm.

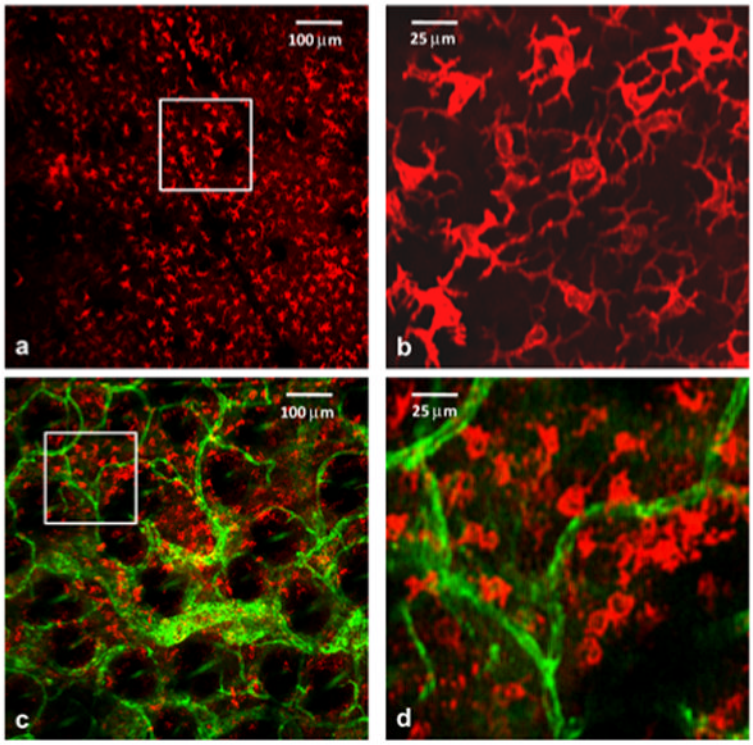

Figure 2.

In vivo confocal fluorescence images of an EMT6 tumor 2 h after intradermal injection with fluorophore-conjugated αMHC-II and αCD31. (a) MHC-II$^+$ cells (red) visualized at a depth of ~ 40 μm in the tumor with morphology consistent with that of Langerhans cells. No CD31-positive vasculature is observed at this depth. (c) Positively stained cells (red) at a depth of ~ 80 μm in the tumor in the presence of a highly vascularized tumor microenvironment. The images (b) and (d) are expanded views of the region of interest indicated by the white box superimposed on (a) and (c), respectively. Imaging experiments were performed in 4 tumor-bearing mice, and the results were found to be reproducible. The field of view in images (a) and (c) is 800 μm × 800 μm, while that in (b) and (d) is 200 μm × 200 μm.